

*In vivo* characterisation of a therapeutically relevant self-assembling  $^{18}\text{F}$ -labelled  $\beta$ -sheet forming peptide and its hydrogel using positron emission tomography

---

O. Morris<sup>1,2\*</sup>, M.A. Elsayy<sup>3,4,5</sup>, M. Fairclough<sup>1,2</sup>  
K.J. Williams<sup>2,6</sup>, A. McMahon<sup>1,2</sup>, J. Grigg<sup>7</sup>, D. Forster<sup>1,2</sup>,  
A.F. Miller<sup>4,8</sup>, A. Saiani<sup>3,4,8</sup>, C. Prenant<sup>1,2</sup>

1. Wolfson Molecular Imaging Centre, The University of Manchester, UK
2. CRUK/EPSRC Imaging Centre in Cambridge & Manchester, The University of Manchester, UK
3. School of Materials, The University of Manchester, UK
4. Manchester Institute of Biotechnology, The University of Manchester, UK
5. School of Pharmacy and Biomedical Sciences, University of Central Lancashire, UK
6. Manchester Pharmacy School, The University of Manchester, UK
7. GE Healthcare, Amersham Place, Little Chalfont Bucks UK
8. School of Chemical Engineering and Analytical Science, The University of Manchester, UK

\*correspondence author: [olivia.morris-2@postgrad.manchester.ac.uk](mailto:olivia.morris-2@postgrad.manchester.ac.uk); 44161 2750041; Wolfson Molecular Imaging Centre, The University of Manchester, UK

This article has been accepted for publication and undergone full peer review but has not been through the copyediting, typesetting, pagination and proofreading process which may lead to differences between this version and the Version of Record. Please cite this article as doi: 10.1002/jlcr.3534

## Abstract

Positron emission tomography (PET) and fluorescence labelling have been used to assess the pharmacokinetics, biodistribution and eventual fate of a hydrogel-forming nonapeptide, FEFKFEFKK (F9) in healthy mice, using  $^{18}\text{F}$ -labelled and fluorescein isothiocyanate (FITC) - labelled F9 analogues. F9 was site-specifically radiolabelled with 2- $^{18}\text{F}$ fluoro-3-pyridinecarboxaldehyde ( $^{18}\text{F}$ FPCA) via oxime bond formation.  $^{18}\text{F}$ FPCA-F9 *in vivo* fate was evaluated both as a solution, following intravenous administration, and as a hydrogel when subcutaneously injected. The behaviour of FITC-F9 hydrogel was assessed following subcutaneous injection.  $^{18}\text{F}$ FPCA-F9 demonstrated high plasma stability and primarily renal excretion;  $^{18}\text{F}$ FPCA-F9 when in solution and injected into the bloodstream displayed prompt bladder uptake ( $53.4 \pm 16.6$  SUV at 20 minutes post injection) and rapid renal excretion, whereas  $^{18}\text{F}$ FPCA-F9 hydrogel, formed by co-assembly of  $^{18}\text{F}$ FPCA-F9 monomer with unfunctionalised F9 peptide and injected subcutaneously, showed gradual bladder accumulation of hydrogel fragments ( $3.8 \pm 0.4$  SUV at 20 minutes post injection), resulting in slower renal excretion. Gradual disaggregation of the F9 hydrogel from the site of injection was monitored using FITC-F9 hydrogel in healthy mice ( $60 \pm 3$  over 96 hours), indicating a biological half-life between 1-4 days. The *in vivo* characterisation of F9, both as a gel and a solution highlights its potential as a biomaterial.

## Introduction

The potential of peptide hydrogels as biomaterials is vast on account of their *in vivo* and *in vitro* potential uses in a variety of biomedical applications. These include their use as scaffolding for 3D cell cultures, tissues engineering and regenerative medicine as well as their use as vehicle for localised drug delivery <sup>[1-6]</sup>. Peptide hydrogels are made of short synthetic peptides composed of either natural or non-natural amino acids that are designed to

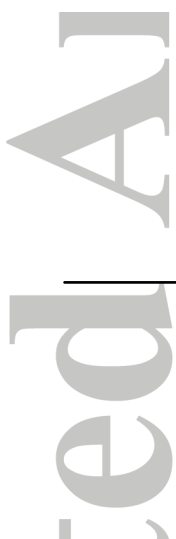
self-assemble into higher biomimetic structures. This is achieved via non-covalent interactions in response to external triggers, such as pH, ionic strength, enzymes and light, to form three-dimensional networks of entangled fibrous structures <sup>[7, 8]</sup>.

In the present study, the *in vivo* behaviour of a  $\beta$ -sheet forming peptide FEFKFEFKK (F9) (F: phenylalanine; K: Lysine; E: glutamic acid) and its hydrogel was characterised. F9 is one of a family of amphipathic peptides with alternating hydrophobic and hydrophilic residues that self-assembles into  $\beta$ -sheet fibres that above a critical gelation concentration (CGC) associates to form a hydrogel. The properties of the hydrogels can be tailored through peptide design, concentration, media pH and ionic strength <sup>[9]</sup>; as such they have been shown to hold promise for application in the biomedical field as 3D cell culture matrices <sup>[10]</sup> and/or drug delivery vehicles <sup>[5]</sup>.

Positron emission tomography (PET) is a quantitative imaging modality boasting high levels of sensitivity. The tool was used to assess the behaviour of radiolabelled F9 (<sup>18</sup>F]FPCA-F9) *in vivo* using C3H mice. [<sup>18</sup>F]FPCA-F9 was first delivered as a solution (concentration below CGC, pH 5.6) into the tail-vein to study the fate of peptide monomer in the blood stream. Subsequently [<sup>18</sup>F]FPCA-F9 was delivered as part of an F9-hydrogel (concentration above CGC, pH 5.6) by co-assembly with unfunctionalised F9 peptide, before subcutaneous injection into the mouse flank.

Site-specific radiolabelling of F9 was selected to safeguard the  $\beta$ -sheet forming and therefore the gel-forming capability of the peptide. To achieve this, the *N*-terminal amine was functionalised with an amino(oxy)-group to give (Aoa)F9 (Mr 1338.59 Da). Functionalisation of the peptide with the amino(oxy)-moiety permits its radiolabelling with the <sup>18</sup>F-prosthetic group 2-[<sup>18</sup>F]fluoro-3-pyridinecarboxaldehyde (FPCA) via oxime-bond formation, as has

radiolabelli



PET studies with [ $^{18}$ F]-fluorescein isothiocyanate provided information on the first 5 days; a time-f

## Experimental

All solvents w

## Experimental

All solvents w

(Aoa)F9 was p

purity >98 %. FITC-F9 was purchased from Biomatik as a TFA salt (purity >98 %) and converted into the HCl salt of the peptide. [ $^{18}\text{F}$ ]Fluoride was produced onsite via the  $^{18}\text{O}(p, n)^{18}\text{F}$  nuclear reaction by 16.4 MeV proton bombardment of enriched [ $^{18}\text{O}$ ]H<sub>2</sub>O using a GE PETtrace cyclotron (GE Healthcare, Sweden). Analytical HPLC was performed using a Shimadzu (Milton Keynes, UK) Prominence system (LC-20AB solvent delivery system, SPD-20A dual wavelength absorbance detector) controlled by LabLogic (Sheffield, UK), Laura 3 software via a CBM-20A controller. HPLC eluate was measured for radioactivity using a Bioscan (Oxford, UK) Flow-count B-FC 3100 gamma detector. All pre-clinical PET scans were carried out using a Siemens (Oxford, UK) Inveon® PET-CT scanner. Fluorescence *in vivo* imaging was carried out using a Biospace Lab Photon Imager Optima (Nesles-la-Valee, France) controlled by Biospace Lab Photo Acquisition software v3.4 and images analysed using Biospace Lab M3 Vision software.

## **Radiochemistry**

### **[ $^{18}\text{F}$ ]Potassium fluoride**

Cyclotron produced [ $^{18}\text{F}$ ]fluoride was delivered to a TRACERlab FX-FN radiochemistry system (GE Healthcare, UK) and trapped on a Sep-Pak QMA cartridge (Oasis, Waters, UK). The cartridge was then eluted with a K<sub>2</sub>CO<sub>3</sub> solution (4  $\mu\text{mol}$ , 0.4 mL) into a reactor containing 18-crown-6 (8 mg, 30  $\mu\text{mol}$ ) in acetonitrile (0.6 mL). The mixture was azeotropically dried with 3 sequential additions of acetonitrile (1.6 mL total) at 90 °C under nitrogen.

### **[ $^{18}\text{F}$ ]FPCA**

[ $^{18}\text{F}$ ]FPCA was produced as per the methodology described by Morris *et al* <sup>[11]</sup>. In short, 3-carboxaldehyde-*N,N,N*-trimethylpyridine-2-aminium bromide (2 mg, 8  $\mu\text{mol}$ ) in DMSO (200  $\mu\text{L}$ ) was added to the reactor containing azeotropically dried [ $^{18}\text{F}$ ]fluoride and heated to 70°C for 10 min. [ $^{18}\text{F}$ ]FPCA was trapped and washed on an AFFINIMIP® (AFFINISEP,

France) 2.0 mL solid phase extraction (SPE) cartridge. Elution of [ $^{18}\text{F}$ ]FPCA was achieved using methanol (3 mL) into the reactor followed by solvent evaporation under vacuum at 60°C for 6.5 min. Synthesis of the 3-carboxaldehyde-*N,N,N*-trimethylpyridine-2-aminium bromide precursor is described elsewhere <sup>[11]</sup>.

#### **[ $^{18}\text{F}$ ]FPCA-F9 solution**

A mixture of (Aoa)F9 (1.5 mg, ~880 nmol), anilinium hydrochloride (2.6mg, 20  $\mu\text{L}$ ) and gentisic acid (sodium salt hydrate, 1 mg) in citric acid (0.02 M, 250  $\mu\text{L}$ ) was added to purified and dried [ $^{18}\text{F}$ ]FPCA (pH 2.7). The reaction mixture was heated to 70 °C for 30 minutes and purified using a TSK-gel® SE-HPLC column (7.5mm ID x 30 cm, 10  $\mu\text{m}$ , Hichrom Tosoh Bioscience, Berkshire UK) eluted with PBS with 1 % ascorbic acid / 1mL/min,  $t_{\text{R}}$  = 10 minutes and analysed for quality control purposes using size exclusion-HPLC (SE-HPLC) (Superdex peptide 10/300 GL, PBS, 1 mL/min, 220 nm,  $t_{\text{R}}$  = 18.05 minutes). The final concentration of the solution was 0.3 mM.

#### **[ $^{18}\text{F}$ ]FPCA-F9 hydrogel**

[ $^{18}\text{F}$ ]FPCA-F9 was prepared as described above. [ $^{18}\text{F}$ ]FPCA-F9 hydrogel was prepared by adding a small amount of [ $^{18}\text{F}$ ]FPCA-F9 to an unlabelled, unfunctionalised F9 hydrogel. In short, unfunctionalised F9 (11.6 mg) in  $\text{H}_2\text{O}$  (440  $\mu\text{L}$ ) was sonicated for 15 minutes before addition of 120  $\mu\text{L}$  (411 nM) of purified [ $^{18}\text{F}$ ]FPCA-F9 in PBS solution. The mixture was vortexed and the pH adjusted to 5.5 using NaOH (0.5 M) and the final volume increased to 600  $\mu\text{L}$  using  $\text{H}_2\text{O}$  giving a final hydrogel concentration 0.01M.

#### **Fluorescence preparation**

##### **FITC-F9 hydrogel**

FITC-F9 hydrogel was prepared using the same procedure as described above. Unfunctionalised F9 (10.5 mg) in  $\text{H}_2\text{O}$  (440  $\mu\text{L}$ ) was sonicated for 15 minutes before addition

of FITC-labelled F9 (1.2 mg) in DMSO (5  $\mu$ L). The mixture was sonicated for a further 15 minutes and the pH adjusted to 5.5 using NaOH (0.5 M). The final volume was increased to 491.5  $\mu$ L using deionised H<sub>2</sub>O giving, once again, a final hydrogel concentration of 0.01M.

### **Pre-clinical analyses**

All animal handling was in accordance with UK legislation under the 1986 Animals (Scientific Procedures) Act.

### **Pre-clinical PET [<sup>18</sup>F]FPCA-F9 solution & hydrogel**

C3H mice were anaesthetised using isoflurane induction 4 % and maintained 1.5 % in 70 % N<sub>2</sub>O and 30 % O<sub>2</sub> mixture. [<sup>18</sup>F]FPCA-F9 solution was injected in the tail vein (13 MBq, n=4) of healthy mice or [<sup>18</sup>F]FPCA-F9 hydrogel was injected subcutaneously into the right flank of different healthy mice (2-5 MBq, n=3). The acquisition protocol parameters consisted of a preliminary CT scan to determine attenuation correction factors followed by a 1 and 4 hour PET acquisition time for [<sup>18</sup>F]FPCA-F9 solution and hydrogel respectively. Major excretory organs, including liver, kidney and bladder as well as bone and hydrogel region (in [<sup>18</sup>F]FPCA-F9 hydrogel scans only), were delineated on CT and uptake was quantified as SUV.

### **[<sup>18</sup>F]FPCA-F9 pre-clinical metabolite analysis**

Plasma, kidney and urine samples were taken post-sacrifice at 5 (n=2) and 20 (n=2) minutes post injection of [<sup>18</sup>F]FPCA-F9 monomer. Plasma was extracted from whole blood samples using a Thermo ALC multispeed refrigerated centrifuge PK121R (8720 g, 4 °C for 3 minutes). Kidney samples were homogenised, centrifuged (8720 g, 4 °C for 3 minutes) and the supernatant removed for HPLC analysis. Urine samples were directly injected onto HPLC without sample preparation using a GE Superdex peptide 10/300 GL (GE Healthcare, UK) eluted with PBS (1 mL/min, 220 nm).

### ***In vivo* fluorescence analysis**

C3H mice (n = 2) were anaesthetised using isoflurane (induction 4 % and maintained 1.5 %) in 70 % N<sub>2</sub>O and 30 % O<sub>2</sub> mixture. FITC-F9 gel (200 µL) was injected subcutaneously into the right flank (C3H mice) and fluorescence data attained over 5 days using a 30 second acquisition time. Relative bioluminescent counts were normalised to acquisition time and quantified in units of counts. Excitation and emission wavelengths 487 and 547 nm respectively, FLI integration at 400 ms per frame, BVR pixel 171 µm with a pixel size of 170 x 170 µm. Hydrogel site was delineated and emission was quantified as counts per minute.

## **Results and Discussion**

### **[<sup>18</sup>F]FPCA-F9 radiochemistry**

The radiochemical conversion of (Aoa)F9 to [<sup>18</sup>F]FPCA-F9 by reaction with [<sup>18</sup>F]FPCA was 63 ± 7 % and 400 ± 200 MBq of [<sup>18</sup>F]FPCA-F9 were produced (decay-corrected from end of bombardment) starting with 25-30 GBq of [<sup>18</sup>F]fluoride (n=6). Radiosynthesis of [<sup>18</sup>F]FPCA-F9 as a solution and a hydrogel was completed within 2 hours from end of bombardment.

Figure A of supplementary material provides GE TRACERlab FX-FN trace for crude reaction mixture. Radiochemical purity of [<sup>18</sup>F]FPCA-F9 >98 % was attained, as can be seen in Figure B of supplementary material. [<sup>18</sup>F]FPCA-F9 radiochemical yields (RCY) were not reflective of the high radiolabelling efficiency of (Aoa)F9 with [<sup>18</sup>F]FPCA, due to significant product loss during the automated radiosynthesis. This was attributable to the agglutinative nature of the peptide and issues of poor solubility and high viscosity of (Aoa)F9, despite using low concentrations; this caused handling difficulties for the automated platform due to the platform's narrow-bore tubing. Notwithstanding, [<sup>18</sup>F]FPCA-F9 was produced in sufficient quantities for use in PET analysis. It is anticipated that use of larger-bore tubing and the ability to transfer the reaction mixture across the platform using a syringe drive, as



opposed to a helium flow, which is slow and controlled might improve recovery of [ $^{18}\text{F}$ ]FPCA-F9. However, the uniquely aggregative nature of the hydrogel-forming peptide precludes its comparison with other [ $^{18}\text{F}$ ]FPCA peptide radiolabelling.

### **[ $^{18}\text{F}$ ]FPCA-F9 solution biodistribution - PET**

The PET images in Figure 2 A, B and C depict [ $^{18}\text{F}$ ]FPCA-F9 biodistribution at 60 seconds, 15 minutes and 1 hour post injection respectively. Figure 2D shows the uptake of [ $^{18}\text{F}$ ]FPCA-F9 over 60 minutes in key organs. Kidney uptake was observed within 5 minutes post injection ( $5.9 \pm 1.9$  SUV).

This was followed by significant bladder accumulation, as clearly seen in Figures 2B and C, which begins to plateau after 20 minutes ( $53.4 \pm 16.6$  SUV). Liver uptake remained low over the time course of the scan ( $1.4 \pm 0.1$  and  $0.7 \pm 0.1$  SUV at 5 and 20 minutes post injection respectively). The concentrations observed within the liver were consistently lower than those seen in the kidney whilst the highest concentration were seen in the bladder; confirming that the kidney is the major excretory organ for [ $^{18}\text{F}$ ]FPCA-F9 and potential radiometabolite(s). Rapid renal excretion is expected of unmodified, small peptides <sup>[12, 13]</sup>.

Gradual bone accumulation can also be seen ( $7.8 \pm 2.5$  SUV 1 hour post injection), although levels of radioactivity are overshadowed by much higher concentrations in the bladder ( $47.4 \pm 7.2$  SUV 1 hour post injection); bone uptake was most notable at regions of the joint. Accumulation of radioactivity in the bone can be ascribed either to defluorination of [ $^{18}\text{F}$ ]FPCA-F9 or to the interaction of the peptide with the bone tissue. Bone uptake followed kidney uptake, an organ which has been previously implicated in defluorination <sup>[14, 15]</sup>, however no free [ $^{18}\text{F}$ ]fluoride was observed in metabolic analyses (discussed later) we cannot, therefore, exclude the possibility of an interaction between a positively charged [ $^{18}\text{F}$ ]FPCA-F9 (at physiological pH) and negatively charged protein rich cartilage tissue.

This potential interaction is currently being investigated in our laboratory and is outside the scope of this article.

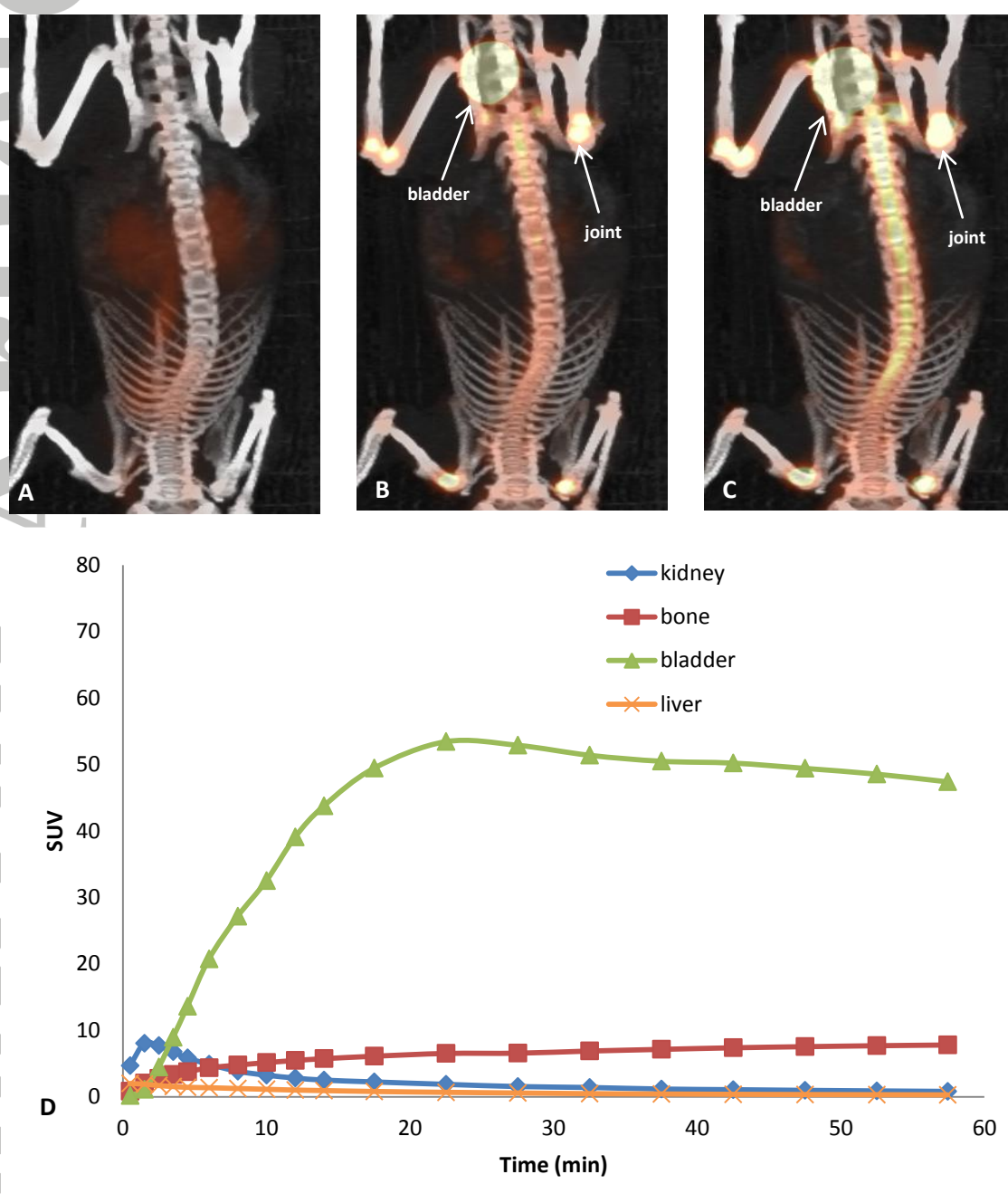


Figure 2:  $[^{18}\text{F}]$ FPCA-F9 solution at A) 60 seconds, B) 15 minutes and C) 1 hour post injection and D) TAC  $[^{18}\text{F}]$ FPCA-F9 biodistribution in bone and excretory organs (C3H mice, n=4)

## **[<sup>18</sup>F]FPCA-F9 solution metabolite analysis**

Liver, kidney, urine and plasma samples were analysed using SE-HPLC to quantify the degree of metabolic degradation of the peptide. The analysis identified the major peak as [<sup>18</sup>F]FPCA-F9 with a retention time of ~18 minutes; none of the samples analysed showed any metabolite of [<sup>18</sup>F]FPCA-F9 (see Supplementary Material Figure C). Table 1 shows the percentage of parent compound ([<sup>18</sup>F]FPCA-F9) identified in each of the samples after 60 minutes. The high percentage of parent compound in all samples demonstrates the high stability of [<sup>18</sup>F]FPCA-F9.

Liver and kidney samples, though, showed a second peak at ~8 minutes accounting for ~5 % of the radioactivity (see Supplementary Material Figure Cii). Urine samples showed a peak with a retention time of ~12 minutes, accounting for 5 % of the radioactivity (see supplementary Figure Ciii) alongside the [<sup>18</sup>F]FPCA-F9 peak. A shorter retention time is suggestive of a larger species than [<sup>18</sup>F]FPCA-F9, conceivably a result of [<sup>18</sup>F]FPCA-F9 aggregation or interaction with a large molecular weight protein. As discussed above, [<sup>18</sup>F]FPCA-F9 carries a positive charge under physiological conditions and can therefore interact with negatively charged proteins. The large molecular weight radiolabelled species seen in both liver and kidney samples ( $t_R$  ~8 minutes), falls outside the exclusion limit of the column ( $V_0$  ~9 minutes) therefore suggestive of molecular mass >12 kDa. The species in the urine sample ( $t_R$  12.5 minutes) is likely, according to molecular weight standard analysis, to have a molecular mass between 8 and 10 kDa.

The absence of radiolabelled species with a molecular mass smaller than that of [<sup>18</sup>F]FPCA-F9 and within the 22.5 minute column exclusion limit is suggestive of the absence of [<sup>18</sup>F]FPCA-F9 radiometabolites, including [<sup>18</sup>F]fluoride. The absence of a [<sup>18</sup>F]fluoride

radiometabolite provides evidence against [ $^{18}\text{F}$ ]FPCA-F9 defluorination and further supports the notions of an interaction between F9 and the cartilage.

If [ $^{18}\text{F}$ ]FPCA-F9 is aggregating with circulating proteins, similar aggregation is expected to be observed in plasma sample, which is not the case. The TAC shows that F9 is rapidly transported to the kidneys, thereby minimising the time for which F9 can interact with circulating proteins such as albumin in the plasma.

*Table 1: Quantification of parent ([ $^{18}\text{F}$ ]FPCA-F9) fraction after 60 minutes (data expressed as mean  $\pm$  SD,  $n=4$ )*

<b>Liver</b>	<b>Kidney</b>	<b>Urine</b>	<b>Plasma</b>
94 $\pm$ 0 %	95 $\pm$ 1 %	95 $\pm$ 1 %	100

Importantly, [ $^{18}\text{F}$ ]FPCA-F9 showed high plasma stability according to metabolite analysis and is rapidly and predominantly excreted by the kidney; thereby showing a favourable biodistribution profile for the use of F9 as a biomaterial.

### **[ $^{18}\text{F}$ ]FPCA-F9 hydrogel biodistribution - PET**

[ $^{18}\text{F}$ ]FPCA-F9 hydrogel was injected subcutaneously into the flank of C3H mice; its *in vivo* behaviour over a 4 hour time-course can be interpreted from Figure 3. Figures 3 A and B (60 seconds and 4 hours post injection) clearly show the radiolabelled hydrogel. Figure 3C provides the biodistribution of [ $^{18}\text{F}$ ]FPCA-F9 peptide in the bone and excretory organs. The increasing concentrations of [ $^{18}\text{F}$ ]FPCA-F9 in the kidneys and bladder clearly show that the peptide is gradually being eluted from the hydrogel as the latter physically degrades / disaggregates.

A progressive increase in radioactivity over 150 minutes is observed in the bladder, before plateauing (17.4  $\pm$  1.3 SUV). Although this is reminiscent of the excretion profile of the peptide solution, albeit over a different time period, there is a two-step profile for bladder

accumulation that was observed in all mice. This is anticipated to be as a result of the staged non-uniform disaggregation of the hydrogel; smaller and more vulnerable hydrogel fragments at the periphery are expected to disaggregate first and rapidly before the bulk of the hydrogel.

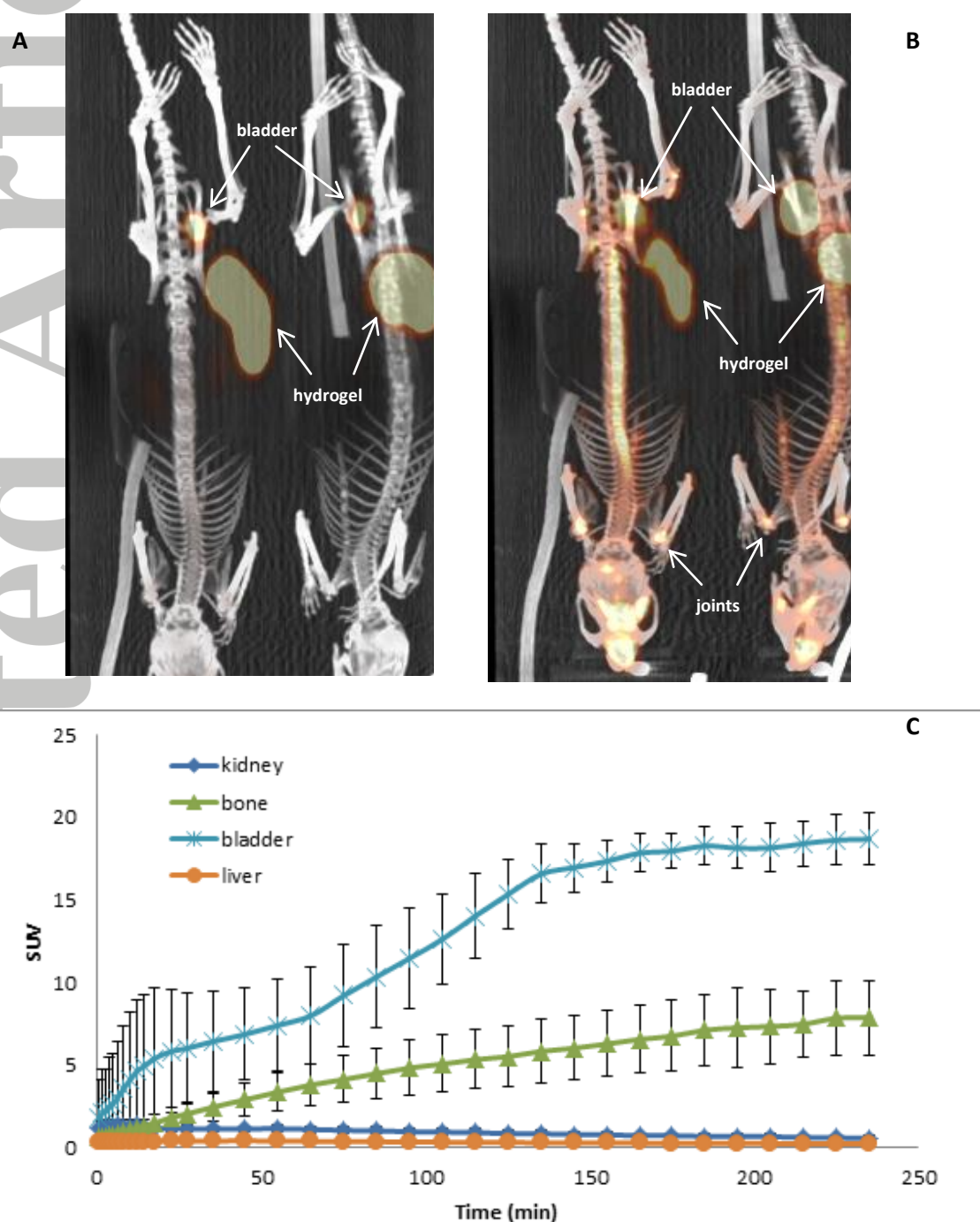


Figure 3: [ $^{18}\text{F}$ ]FPCA-F9 hydrogel at A) 60 seconds and B) 4 hours post injection C) TAC showing [ $^{18}\text{F}$ ]FPCA-F9 biodistribution in bone and excretory organs (C3H mice,  $n=3$ )

Bone uptake of [ $^{18}\text{F}$ ]FPA-F9 was also observed ( $3.8 \pm 1.3$  SUV 1 hour post injection) in this case and can be seen in Figure 3. Uptake of [ $^{18}\text{F}$ ]FPCA-F9 in the kidney, bladder and liver, major excretory organs, ( $1.15 \pm 0.2$ ,  $5.9 \pm 3.8$  and  $0.4 \pm 0.1$  SUV respectively, 20 minutes post injection) and also shown in Figure 3C. Akin to when [ $^{18}\text{F}$ ]FPCA-F9 was administered as a solution, liver uptake remained below the levels observed in the kidney and significantly below bladder levels and this was true over the duration of the experiment ( $0.7 \pm 0.1$  SUV at 20 minutes post injection). The work confirms that the peptide exhibited the projected biodistribution with no significant changes in its *in vivo* behaviour, on account of its gelation.

### **FITC-F9 hydrogel - fluorescence imaging**

Despite the inability to detect FITC-F9 penetration into the tissue, as a consequence of the limitations imposed by FITC emission, shallow injection of FITC-F9 produced fluorescence data that was a good indicator of the hydrogel biological half-life. The intention of using BLI as a complementary technique was to help visualise the process of hydrogel expansion and disaggregation; this data was used to augment PET data which was used to provide information regarding biodistribution and route of F9 metabolism.

Fluorescence data is presented in Figure 4, the data shows FITC-F9 hydrogel 60 seconds, 48 and 96 hours post injection (Figure 4 A, B and C respectively) in the flank of C3H mice (n=2).

Qualitative analysis of the preliminary data permits a first appreciation of the results. Signal intensity, corresponding to FITC-F9, was measured over the course of 5 days, beginning at the time of injection. Steady depletion in signal intensity was observed, with a  $43 \pm 8$  % reduction over the first 24 hours and  $60 \pm 3$  % over 96 hours, attributable to disaggregation of the hydrogel over time. Results of the fluorescence work, therefore, suggest an F9 hydrogel biological half-life between 1 and 4 days.



An expansion of ~10 % was observed over the first 24 hours, which dropped to ~3 % over 48 hours. These results suggest that, post injection, there is further penetration of the hydrogel in the surrounding tissues. These hydrogels are known to be shear thinning and animal movement will promote gel tissue penetration. This is then followed by the slow disaggregation of the hydrogel.

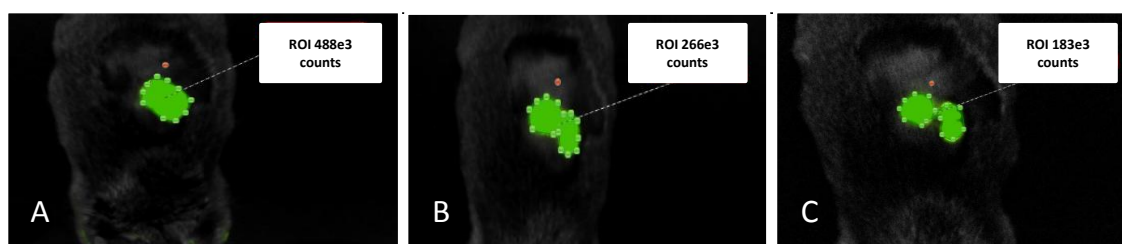


Figure 4: Fluorescence imaging of FITC-F9 hydrogel A) 60 seconds, B) 48 hours and C) 96 hours post injection

The fluorescence data, despite not being fully quantitative, are in agreement with PET data providing evidence for the exploitable *in vivo* life-time of F9 hydrogels as a biomaterial for either tissue engineering or drug delivery applications.

## Conclusion

We report the automated synthesis of a radiolabelled gel-forming peptide, [ $^{18}\text{F}$ ]FPCA-F9, and its pre-clinical PET analysis alongside preliminary fluorescence imaging data; this permitted *in vivo* characterisation of its behaviour. Pre-clinical results demonstrated renal excretion as the major elimination route for labelled-F9 monomer, both after administration as a solution and a hydrogel. Results also showed the high plasma stability of the labelled-F9 monomers and established a favourable biological half-life of labelled-F9 hydrogel. The current work has confirmed that the behaviour exhibited by F9 is typical of natural, small peptides<sup>[12]</sup> and its *in vivo* biodistribution is not altered on account of its gel-form.

Collectively, the fluorescence and PET data provide insight into a possible *in vivo* pathway for F9 hydrogel; firstly characterised by hydrogel tissue penetration followed by disaggregation and final elimination via renal excretion. Due to the natural amino acid composition of F9 alongside its *in vivo* metabolic profile, F9 is not expected to have issues of toxicity<sup>[16]</sup>. Such characteristics would highlight F9 hydrogel as ideal biomaterial that could be used as a silent carrier for localised drug-delivery. This is of particular importance in oncological applications wherein targeted drug delivery helps to ensure maximal drug dose at the tumour whilst minimising drug delivery to non-target sites.

### **Disclosure statement**

The authors declare no potential sources of conflict of interest or competing financial interest.

### **Acknowledgements**

We gratefully acknowledge the EPSRC (Fellowship Grant No. EP/K016210/1) for funding the work. OM, AM, KJW and CP gratefully acknowledge the support of the MRC and GE Healthcare for funding OM studentship [Grant no. MR/J012521/1] as well as the support of the Cancer Imaging Centre in Cambridge and Manchester (CRUK/EPSRC [C8742/A18097]). The authors would like to thank The Manchester Institute of Biotechnology and School of Materials as well as The Wolfson's research, radiochemistry and pre-clinical teams, in particular A. Smigova for their support with pre-clinical PET. All research data supporting this publication are directly available within this publication and its associated supplementary information.



## References

- [1] A. Mujeeb, A. F. Miller, A. Saiani, J. E. Gough, *Acta Biomaterialia* **2013**, 9, 4609.
- [2] S. Wan, S. Borland, S. M. Richardson, C. L. R. Merry, A. Saiani, J. E. Gough, *Acta Biomaterialia* **2016**, 46, 29.
- [3] L. A. Castillo Diaz, A. Saiani, J. E. Gough, A. F. Miller, *Journal of Tissue Engineering* **2014**, 5, 2041731414539344.
- [4] L. A. Castillo Diaz, M. Elsayy, A. Saiani, J. E. Gough, A. F. Miller, *Journal of Tissue Engineering* **2016**, 7, 2041731416649789.
- [5] C. Tang, A. F. Miller, A. Saiani, *International Journal of Pharmaceutics* **2014**, 465, 427.
- [6] D. Roberts, C. Rochas, A. Saiani, A. F. Miller, *Langmuir* **2012**, 28, 16196.
- [7] A. Dasgupta, J. H. Mondal, D. Das, *RSC Advances* **2013**, 3, 9117.
- [8] A. M. Jonker, D. W. P. M. Löwik, J. C. M. van Hest, *Chemistry of Materials* **2012**, 24, 759.
- [9] M. A. Elsayy, A. M. Smith, N. Hodson, A. Squires, A. F. Miller, A. Saiani, *Langmuir* **2016**, 32, 4917.
- [10] L. Szkolar, J.-B. Guilbaud, A. F. Miller, J. E. Gough, A. Saiani, *Journal of Peptide Science* **2014**, 20, 578.
- [11] O. Morris, J. Gregory, M. Kadirvel, F. Henderson, A. Blykers, A. McMahon, M. Taylor, D. Allsop, S. Allan, J. Grigg, H. Boutin, C. Prenant, *Applied Radiation and Isotopes* **2016**, 116, 120.
- [12] L. Di, *The AAPS Journal* **2015**, 17, 134.
- [13] T. Katsila, A. P. Siskos, C. Tamvakopoulos, *Mass Spectrom Rev* **2012**, 31, 110.
- [14] E. D. Kharasch, D. C. Hankins, K. E. Thummel, *Anesthesiology* **1995**, 82, 689.
- [15] T. L. Chen, T. G. Chen, Y. T. Tai, H. C. Chang, R. M. Chen, C. J. Lin, T. H. Ueng, *Can J Anaesth* **2000**, 47, 680.
- [16] M. P. Hall, *Drug Metab Dispos* **2014**, 42, 1873.